DISPERSION OF NANOCLAY IN 1,4-POLYBUTADIENE

G. MONTELLA,[1] A. P. PURDY,[1] S. B. QADRI,[2] N. BHATTARAI,[2] R. M. STROUD,[2] C. M. ROLAND[1,*]

[1]CHEMISTRY DIVISION AND

[2]MATERIALS SCIENCE AND TECHNOLOGY DIVISION, NAVAL RESEARCH LABORATORY, WASHINGTON, DC 20375-5342

RUBBER CHEMISTRY AND TECHNOLOGY, Vol. 91, No. 4, pp. 633–643 (2018)

ABSTRACT

Two approaches to obtaining better dispersion of organo-modified nanoclay in high-molecular weight polybutadiene were assessed: (1) chemical modification of the polymer to increase its affinity for the silicate layers and (2) increasing the stretching component of the flow field used to mix the materials. As expected, the degree of dispersion, that is, the extent of intercalation of the polymer into the clay galleries and amount of exfoliation of the clay layers, increased with closer matching of the respective solubility parameters of the components. The efficiency of mechanical mixing was greater for flow fields dominated by stretching (extensional flow); less mix energy had to be expended to achieve a given level of reinforcement. However, without sufficient affinity of the polymer for the clay, complete exfoliation could not be obtained solely by mixing. Nevertheless, incomplete dispersion of the nanoclay still yields more than 40-fold increases in viscosity with 5% clay. [doi:10.5254/rct.18.81567]

INTRODUCTION

The appeal of nanoparticle reinforcement of polymers is the potential to effect large property changes with small filler concentrations. For organo-modified nanoclays, improvements in many physical and mechanical properties,[1,2] including barrier performance,[3,4] thermal stability,[5] and fire retardancy,[6] have been reported. However, there is a well-recognized problem in exploiting this potential: the difficulty of achieving sufficient dispersion of the particles.[7,8] This problem is inherent to nanocomposites; that is, the enormous surface area that gives rise to property enhancements also drives agglomeration of the particles. Mixing methods including ultrasonic agitation, along with the use of solvents, are popular methods of dispersing nanoparticles. For nanoclays, the affinity of the matrix material for the clay influences the capacity of polymer chains to intercalate the silicate layers.[1,9–14] Generally, it has been found that satisfactory dispersions of nanoclay are limited to polar, low-molecular-weight polymers.

In this work, we employ two approaches to dispersing organo-modified nanosilicates in high-molecular-weight 1,4-polybutadiene (BR). First, the polarity of the polymer is systematically varied by chemical modification, specifically, introduction of oxirane moieties in the backbone to enhance compatibility with the clay. Second, we varied the flow field to introduce more stretching and less shearing. Extensional flow is the strongest of flow types, that is, the most effective at orienting and fracturing dispersed domains.[15–17] Shear flow, which combines stretching and rotation, is less efficient because the rotational component counters elongational forces as the dispersed particle reorients. For this reason, shear fields lack persistence of the strain history.[18,19] Previously, some success has been reported for dispersing polymer nanocomposites by improving compatibility in combination with appropriate mixing methods.[20–22] We found herein that greater affinity of the polymer for the clay increased intercalation but was insufficient to completely exfoliate the clay. The dispersion was significantly improved by further mechanical mixing, with extensional flow significantly more efficient than shear flow. However, if compatibility is poor, exfoliation solely by mixing was not obtained.

*Corresponding author. Email: roland@nrl.navy.mil

TABLE I
POLYMERS

Sample	Epoxidation (by wt.)	T_g, C	δ, $MPa^{1/2}$
BR	0%	−99.5 °C	6.5
EBR15	14.9%	−89.3 °C	7.6
EBR30	29.0%	−69.6 °C	8.7
EBR50	46.6%	−53.6 °C	10.2

EXPERIMENTAL

SAMPLE PREPARATION

The polymer was 1,4-polybutadiene (9.3 ± 0.2% vinyl content) with an average molecular weight of 138.3 kDa. Epoxidation (Table I) was carried out by adding aqueous peracetic acid (Aldrich, 39%) in dichloromethane, dropwise to a dichloromethane solution of the BR (0.04 g/mL). To illustrate, in one preparation (EBR50), 7.21 g of the peracetic acid solution was mixed with 103 g CH_2Cl_2 and added to 4.02 g BR dissolved in 157 g CH_2Cl_2. The reaction was carried out in an ice bath for 16 h. To remove unreacted acid, the mixture was washed 20–30 times with water, followed by several washings with a 0.1 M $NaHCO_3$ solution and a final rinse with water. Residual water was removed by freezing the solution at −25 °C and filtering. The epoxidized polymer was then dried using a rotary evaporator, continued overnight under vacuum to remove residual solvent.

The extent of epoxidation was determined from proton NMR spectra of deuterated chloroform solutions. Unmodified 1,4-polybutadiene has alkene proton resonances at 5.37 and 4.95 ppm, a methylene peak at 2.013 ppm, and methine and methyl (the latter from branched or end groups) resonances falling between 1.2 and 1.6 ppm. We measured 0.54 for the ratio of the integrated intensity of the alkene and aliphatic protons, close to the theoretical value of 0.50. Epoxidation diminishes the alkene peaks, with two new, isolated proton peaks appearing at 2.90 and 2.65 ppm; these are due to the oxirane moiety. In addition, new aliphatic peaks appear between 1 and 2 ppm, overlapping to some extent the CH_2 peaks. The degree of epoxidation was determined as the ratio of the integrated epoxy proton intensity to the summed intensities of the epoxy and alkene protons. For the highest epoxidation level, this ratio equaled 46.6%.

The calorimetric glass transitions, measured at 10 K/min, are included in Table I, along with solubility parameters calculated assuming additive group contributions, using data from ref 23.

The clay used in this study is Cloisite 15A, a substituted dimethyl dihydrogenated tallow montmorillonite, supplied as a free-flowing powder by Southern Clay Products, Inc. (Gonzales, TX, USA). It is synthesized by ion-exchanging sodium montmorillonite clays, cation-exchange capacity (CEC) of 0.92–0.95 mequiv/g, with a dimethyl dihydrogenated tallow (di-tallow) ammonium (CEC = 1.25 mequiv/g).[24] The surfactants on this clay are a mixture of dimethyl di-tallow ammonium with aliphatic carbon chains of various lengths. Based on the structure, we calculate $\delta = 9.35\ MPa^{1/2}$, which falls within the range of literature values (8.80–13.69 $MPa^{1/2}$).[25,26]

To incorporate the clay into the BR, the polymer was dissolved in chloroform (1:4 wt/v), after which 5% of the Cloisite 15A, previously dispersed in chloroform and sonicated for an hour, was added. This mixture was gently stirred overnight, followed by drying in a rotary evaporator at room temperature.

Extrusion experiments employed a capillary rheometer (Instron 3211) operating at a constant speed of 254 mm/min at 30 °C. Two dies were used, having the same converging angle but different lengths (Figure 1). The number of passes through the dies is designated in the sample code (e.g., EBR30_50 refers to 50 passes of EBR30).

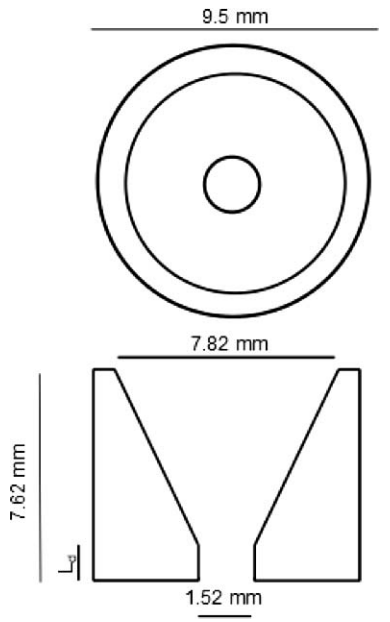

FIG. 1. — Die geometries; $L_d = 1.3$ or 18 mm.

CHARACTERIZATION

Rheology. — The rheological measurements were performed on a strain-controlled rheometer (Anton Paar MCR 502) using parallel plate geometry. Annular samples with an outer diameter of 25 mm and an inner diameter of 19 mm were used so that the strain was more uniform through the material. Preconditioning prior to data acquisition was carried out by imposing an oscillatory strain sweep at 1 rad/s up to 5% strain, followed by a 600 s recovery time. Data were then collected at frequencies between 0.01 and 100 rad/s at 0.5% shear strain (linear viscoelastic region).

Wide-Angle X-Ray Diffraction. — WAXD experiments employed an 18 kW rotating anode instrument (Cu Kα; wavelength = 0.154 nm). Disks, approximately 1 mm thick and prepared by compression molding, were measured in the range $0.1° \leq 2\theta \leq 10°$ at 0.5 °/min.

Transmission Electron Microscopy. — A JEOL JEM2200FS transmission electron microscope (TEM), operated at 200 kV, was used to obtain high-resolution bright-field images. The images were recorded with a Gatan OneView camera, calibrated using a Microcal Si/Ge cross-section standard. TEM samples were prepared by drop casting a suspension (EBR30_50 and EBR30_500) onto a lacey carbon film–coated copper mesh grid.

RESULTS AND DISCUSSION

EFFECT OF EPOXIDATION ON CLAY DISPERSION

The polarity of the interlayer regions of the clay enhances the intercalation of polar polymers.[27,28] Without mechanical mixing, dispersion relies on diffusion of the polymer chains to overcome the platelet adhesion, ultimately leading to platelet separation when sufficient polymer has entered the galleries. In the absence of mechanical stress, this mechanism relies entirely on attractive interactions between the polymer and the clay surface.[27,28] Figure 2 shows the X-ray diffraction (XRD) measured for the nanocomposite of polybutadiene having different levels of

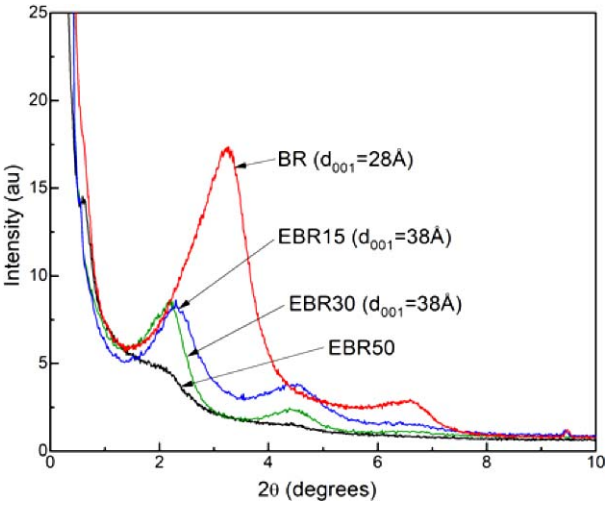

FIG. 2. — XRD of nanocomposites.

epoxidation. For the nonpolar BR, the d spacing (d_{001}) is 28Å. Epoxidation increases the diffraction angle, reflecting greater intercalation (d_{001} = 38Å). The peak intensity is weaker for EBR30 than for EBR15, and for EBR50, there is only a very weak peak; the diffraction angles are all essentially the same. The implication is that exfoliation of the clay increases with epoxidation, although some intercalated structure remains.

This conclusion is supported by the viscosity data in Figure 3. The measurements were made at $T = T_g + 100$, in order to minimize any effect of differences in local friction factor due to the expoxidation.[29] This T_g effect alone changes the viscosity by less than 20%,[29] and the values in Figure 3 were corrected for this. It can be seen that greater exfoliation gives rise to a systematic increase, with a 10-fold increase for the 50% epoxidized polymer. The viscosity enhancement is independent of frequency over this range, although at a sufficiently high strain rate (or at lower temperatures), a greater contribution of segment orientation would reduce the apparent reinforcement (smaller hydrodynamic effect).[30]

EFFECT OF MIXING ON CLAY DISPERSION

An objective of this work was to assess the role of flow field type on dispersion of the clay. The previous section showed that intercalation and exfoliation are promoted by modifying the polymer to increase its affinity for the clay. We expect dispersion to be enhanced as well by subjecting the nanocomposite to an external flow of sufficient strength. In this section, we address the mechanism of delamination of the silicate layers and the conditions required to achieve their separation.

Silicate Layer Interactions. — The clay particles have a size between 6 and 13 μm[24] and are composed of stacked platelets separated by an interlayer that gives rise to the diffraction peaks in Figure 2. The platelets can be separated by rupture, erosion, or peeling, all of which require forces from the surrounding polymer to exceed the layer adhesion. Borse and Kamal[31] estimated the stress required for exfoliation of the clay in polymer nanocomposites. From their analysis, they concluded that the clay particles during flow are broken by a peeling mechanism, since the rupture stress ($\cong 10^7$ Pa for a gallery spacing 1–4 nm) is much larger than the available stresses ($\cong 10^5$ Pa). The adhesive energy per unit crack extension, G, is given by[31]

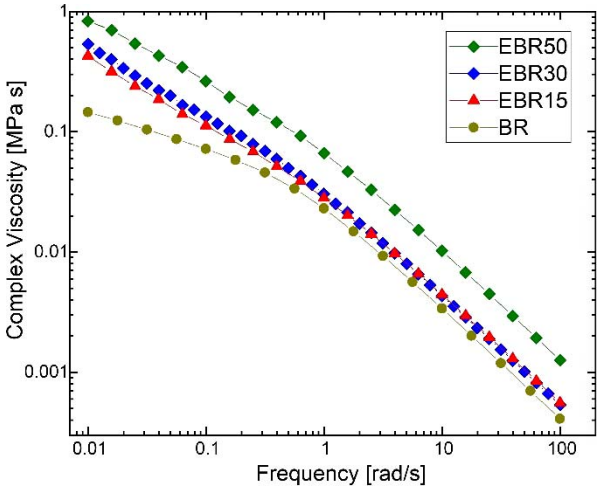

FIG. 3. — Complex viscosity of nanocomposites measured 100° above their respective T_g. Small adjustments (<20%) were made to account for the effect of epoxidation on the neat polymer.

$$G = \frac{F}{b}(1 - \cos\theta)\frac{F^2}{2Etb^2} \tag{1}$$

and the interaction energy U is[32]

$$U = -\frac{A}{12\pi}\left[\frac{1}{d^2} + \frac{1}{(d+t)^2} + \frac{2}{(d+t^2)}\right] \tag{2}$$

where F is the applied force, E is the Young's modulus of the clay platelet, A ($\cong 3.1 \times 10^{-21}$ Nm) is the effective Hamaker constant for organically modified clay platelets,[31] θ is the peel angle, and t and b are the respective thickness and width of the clay platelets, respectively (Figure 4). At equilibrium, $G = U$, and peeling commences when $G > U$. By combining Eqs. 1 and 2, F at equilibrium can be estimated, and the critical shear stress for peeling is

$$\sigma_p = \frac{F}{bl} \tag{3}$$

with l the length of the platelet.

It is difficult to determine the geometry of a single clay platelet. Bandyopadhyay et al.[33] estimated $t = 0.84$ nm and $E = 170$ GPa.[33] Increases in d, b, and l would facilitate separation. Assuming no interaction between the polymer and clay particles (zero peel angle), for $d = 1.44$ nm, they determined the stress required to initiate peeling to be 390 kPa.[33] We assume the same particle geometry, but take $d = 2.8$ nm, which gives a smaller estimate, $\sigma_p = 200$ kPa.

Hydrodynamic Stress during Flow. — Knowing the stress to peel clay particles during flow, it is necessary to assess the hydrodynamic stress exerted on a particle. The Reynolds numbers are given by

$$\mathrm{Re} = 2Q\rho/\pi r\eta \tag{4}$$

For our experiments, $r = 0.038$ mm, $\rho = 0.9$ g/mL, and the volume flow rate is $Q = 18$ mL/s. From the η in Figure 3, $\mathrm{Re} \leq 10^{-5}$. This is several orders of magnitude smaller than the value for turbulence.

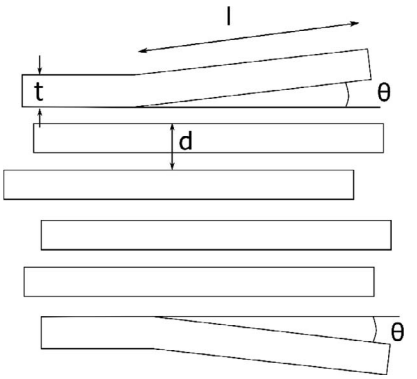

FIG. 4. — Peeling mechanism.

On entry to the capillary, the flow is axisymmetric, with extensional straining along the centerline that becomes simple shear flow near the walls. The velocity gradient tensor can be decomposed into a symmetric and an antisymmetric part; the first represents the vorticity tensor, $\mathbf{\Omega}$, causing particle rotation, and the second corresponds to the rate of strain tensor, $\mathbf{E}$, which deforms the particles. $\mathbf{E}$ can be orthogonally diagonalized, where the diagonal components equal the eigenvalues of $\mathbf{E}$, such that $\lambda_1 > \lambda_2 > \lambda_3$ (indices refer to three orthogonal directions). The maximum positive eigenvalue of $\mathbf{E}$, λ_1, represents the largest elongational velocity gradient. For axisymmetric extensional flow $2\lambda_1 = -\lambda_2 = -\lambda_3$, while for shear flow $\lambda_1 = -\lambda_2$ and $\lambda_3 = 0$. Assuming spherical particles, the mean hydrodynamic stress, σ_h, is given by

$$\sigma_h = \frac{5}{2}\eta\lambda_1 \tag{5}$$

Equation 5 represents the hydrodynamic stress averaged over the hemisphere of a smooth, impermeable particle in a linear flow and oriented to maximize σ_h.[34,35] In adopting this model, we overestimate the stress acting on the clay platelets; moreover, its magnitude varies locally, depending on the surface area of the fragment exposed to the flow. We neglect fluid permeation through the outer regions of the particulate, which would also influence the spatial distribution of the hydrodynamic stresses.

Fluid Dynamic Simulations. — The flow field in the capillary entrance was characterized using a two-dimensional axisymmetric simulation. Considering the characteristics of the polymer flow in the die, the following assumptions were made:

1. Incompressible, laminar flow that is steady state (no variation with time)
2. No slip at the die wall
3. Inertial and gravitational effects are negligible

The flow fields are obtained by solving numerically the equations of motion coupled with the continuity equation, using the finite element code CFD (Comsol 5.2a). In all simulations, the geometry is as given in Figure 1. The non-Newtonian behavior of the polymer was modeled with the Carreau-Yasuda equation[36]

$$\eta = \eta_\infty + (\eta_0 - \eta_\infty)\left[1 + (\tilde{\tau}\dot{\gamma})^2\right]^{\left(\frac{n-1}{2}\right)} \tag{6}$$

fit to the experimental data. In this equation, η_0, η_∞, $\tilde{\tau}$, and n are material constants, with the

TABLE II
CARREAU-YASUDA PARAMETERS FOR EBR30 AT 30 °C

Sample	η_0, MPa s	η_∞	$\tilde{\tau}$, s	n
BR	0.1	0	8.2	0.35
EBR30	0.7	0	192	0.38

obtained values in Table II. Note the time constant of the model is of the same order of magnitude as the reciprocal shear rate at which the polymer becomes non-Newtonian.

The simulation indicates that the available stress during extrusion of the BR is lower than the magnitude necessary to induce delamination of the clay particles, at least assuming no affinity of the polymer chains for the particles, as expected in the absence of epoxidation. For the epoxidized polymers, the required stress is reduced, due to attractive interactions, reflected in the closer equivalence of the solubility parameters (Table I). This promotes intercalation even in the absence of flow (Figure 2). An additional factor that favors better dispersion for the modified polymers is their higher viscosity (Figure 3), which increases hydrodynamic stresses during extrusion (Eq. 5).

As illustrated in Figure 5, the largest stresses are along the flow direction in proximity to the capillary entrance; these correspond to the regions with the highest probability for peeling of the clay layers. However, there is substantial variation across the die radius, as shown in Figure 6 for the BR and EBR30. The largest drag stress occurs in the center of the capillary entrance.

Dispersion Results. — Without mechanical mixing, EBR30 intercalates the clay galleries, but there is minimal exfoliation (Figure 2). This sample was extruded using the dies shown in Figure 1. To maximize the elongational component of the flow, 10 dies were stacked in tandem, so that a single pass subjected the material to repeated converging flow. The length of the dies governed the amount of shear flow. Since the volume over which $\sigma_h > \sigma_p$ is a small part of the total, not all material experiences flow sufficiently strong to effect exfoliation for a given pass. Thus, EBR30 was extruded through the tandem dies as many as 500 times, with randomization between passes.

Shown in Figure 7 are representative XRD traces of the samples subjected to the different extents of mixing. The intensity of the diffraction peak at $2\theta = 2.14°$, which corresponds to $d = 38$ Å, is reduced with increasing mixing level, although all samples exhibited this peak; that is, some

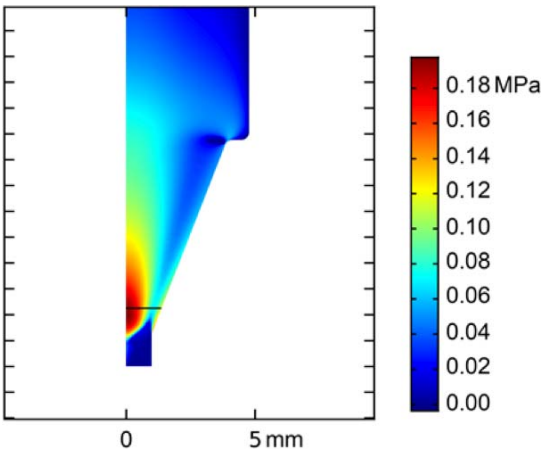

FIG. 5. — Contour plot of hydrodynamic stress (Eq. 5). For the epoxidized polybutadienes, stress distributions are identical but absolute values higher (e.g., by a factor of ~10 for EBR30).

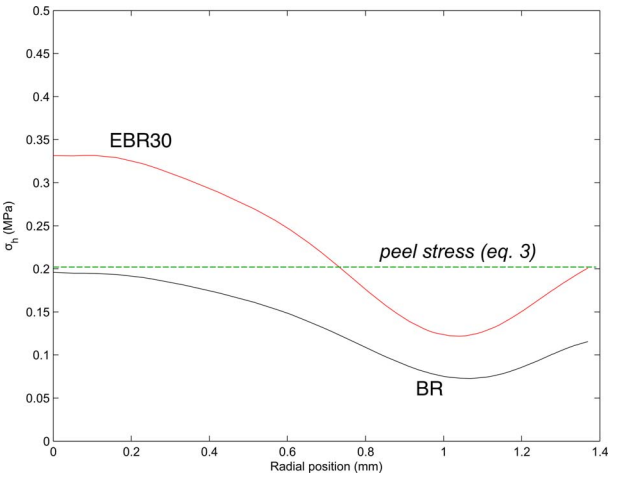

FIG. 6. — Hydrodynamic stress distribution across die near the capillary entrance, at the position of maximum stress. The origin corresponds to the die center.

intercalated clay remained. The increasing extent of exfoliation is associated with higher viscosity (Figure 7, inset).

Figure 8 shows the TEM micrographs obtained for EBR30_50 (left frame) and EBR30_500 (right frame), respectively. The dotted square region on the left frame is magnified in the inset, showing the interplanar spacing of 2.84 nm, similar to the pristine clay as received. On the other hand, the distances between the clay layers are about 44 nm (indicated by arrows in the figure), reflecting exfoliation of the clay. Thus, both pristine and exfoliated clays are present (arrows in the left frame). In addition, intercalated clays with exfoliated clays are seen in in the right frame (indicated by arrows). The fast Fourier transform of a selected region is displayed in the inset. The reflection corresponds to the interplanar spacing of 3.9 nm, due to intercalated clay.

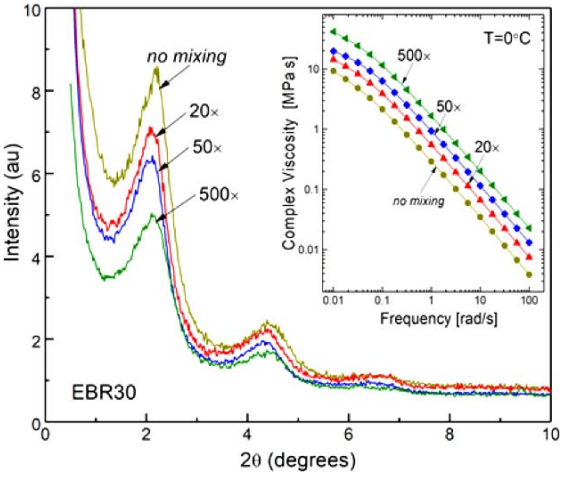

FIG. 7. — XRD of EBR30 after the indicated passes (zero to 500) through the multidie extruder. Inset shows the corresponding viscosities.

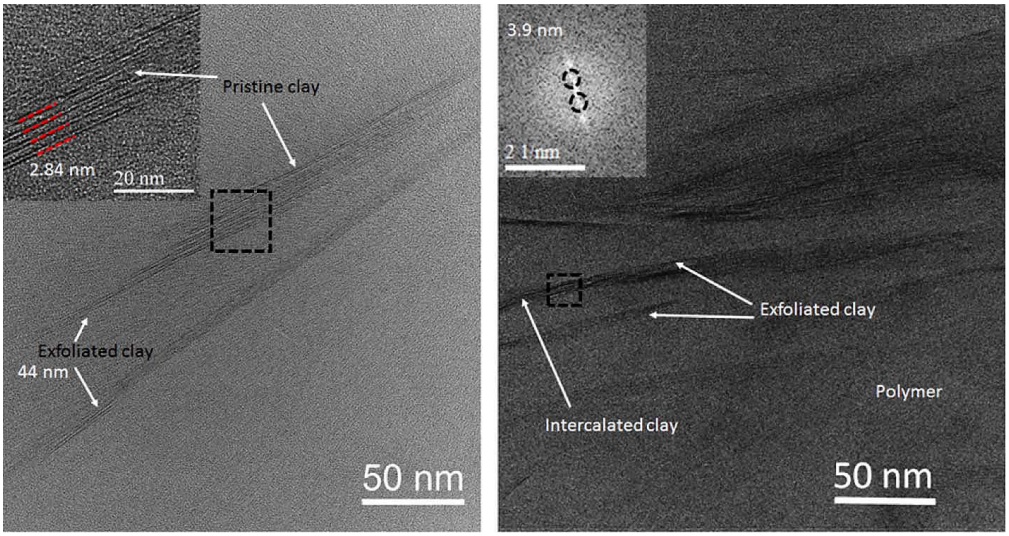

FIG. 8. — (Left) High-resolution TEM of EBR30_50 showing the intermixing of pristine clay and exfoliated clay. The distance measured between the two clay layers was 44 nm, consistent with exfoliation. Inset is the selected region (indicated by box) of the image showing interplanar spacing = 2.84 nm, corresponding to the pristine clay. (Right) TEM for EBR30_500 showing exfoliated clay and intercalated clay layers. Fast Fourier transform of the selected region (box) is displayed in the inset and marked by dotted black circles. Reflection points correspond to interplanar spacing of 3.9 nm, suggesting intercalation of the clay.

Thus, the TEM images show the presence of delaminated platelets, along with intercalated structures; this hybrid morphology is consistent with the XRD in Figure 7. The amount of intercalated clay was reduced with the extent of mixing, with few such structures apparent for EBR30_500. It is interesting to note that despite the fact that simulations show that sufficient flow stress is available to exfoliate the clay, intercalated structures remain. In addition to the fact that, as discussed in the "X-Ray Diffracton" section above, simulations overestimate the stress acting on the clay, the particles remain intact if they do not pass through the region of highest hydrodynamic stress. For this reason, multiple passes through the die are required to increase the probability that any given particle experiences the requisite stress.

Mixing Efficiency. — The mixing efficiency was compared for the two dies differing in capillary length (Figure 1). Since the maximum stress for peeling the layers is at the die entrance, while within the die the stress is lower and mainly shearing, we anticipate a short die to provide more energy efficient dispersion of the clay. The energy density of mixing is proportional to the number of passes, N, through the die times the pressure drop. In Figure 9, the clay dispersion for EBR30, evaluated as the increase in viscosity relative to the composite with no mixing, is plotted versus this specific energy of mixing. For the short die ($L_d = 1.3$ mm in Figure 1), $N \leq 500$, and for the longer die ($L_d = 18.0$ mm), $N \leq 100$. The results demonstrate the significantly higher efficiency of mixing that is more dominated by pure straining flow; that is, less energy is expended on inefficient shear flow.

CONCLUSIONS

In the absence of mechanical mixing, the degree of intercalation of the high-molecular polybutadiene into the galleries of organo-modified clay was governed by the mutual affinity of the two materials. Epoxidation of the polymer to match the solubility parameter of the clay significantly

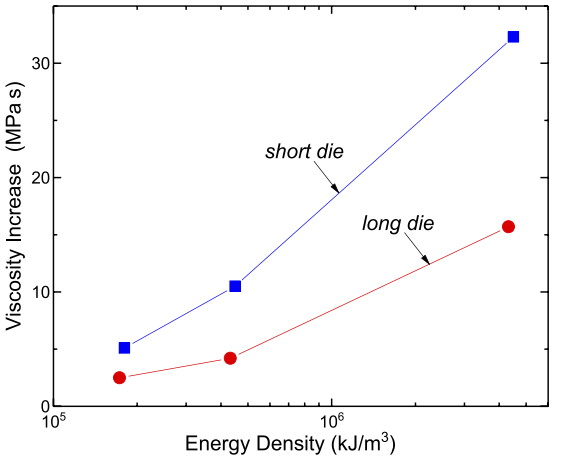

FIG. 9. — Increase in nanocomposite viscosity after repeated passes through the tandem dies, with $z = 1.3$ mm (squares) and 18.0 mm (circles).

increased intercalation and promoted some exfoliation. This greater reinforcement yielded an order of magnitude larger viscosity.

When mechanical mixing was used to disperse the clay, a given degree of intercalation could be achieved at lower mix energies for a flow field dominated by stretching (extensional flow). However, at least for this high-molecular-weight polymer, complete exfoliation was not obtained. Nevertheless, substantial reinforcement can be achieved, with viscosity increases of at least 40-fold for 5% by weight of the nanoclay. This approach can be exploited in an industrial process by augmenting the extensional flow through suppression of shear flow, achieved by debonding the flowing polymer from the walls of the mixer or extruder. Methods to do this include lubrication of the walls[19,37] or the use of ultrasound.[38–40]

ACKNOWLEDGEMENTS

This work was funded by the Office of Naval Research, in part by Code 332 (R. Barsoum, Materials Science Division). G.M. and N.B. acknowledge postdoctoral fellowships from the American Society for Engineering Education and the National Research Council, respectively. We thank Terry Hogan of Firestone Polymers for providing the polybutadiene.

REFERENCES

[1]S. Pavlidoua and C. D. Papaspyrides, *Prog. Polym. Sci.* **33**, 1119 (2008).

[2]M. Kotal and A. K. Bhowmick, *Prog. Polym. Sci.* **51**, 127 (2015).

[3]M. A. Priolo, D. Gamboa, K. M. Holder, and J. C. Grunlan, *Nano Lett.* **10**, 4970 (2010).

[4]M. A. Osman, V. Mittal, M. Morbidelli, and U. W. Suter, *Macromolecules* **37**, 7250 (2004).

[5]S. Sadhu and A. K. Bhowmick, RUBBER CHEM. TECHNOL. **76**, 860 (2003).

[6]W. H. Awad, C. Nyambo, S. Kim, R. J. Dinan, J. W. Fisher, and C. A. Wilkie, "Development of Polyurea Nanocomposites with Improved Fire Retardancy," in *Fire and Polymers V: Materials and Concept for Fire Retardancy*, American Chemical Society, Washington, DC, 2009.

[7]S. K. Kumar, B. C. Benicewicz, R. A. Vaia, and K. I. Winey, *Macromolecules* **50**, 714 (2017).

[8]M. Peplow, *Nature* **503**, 327 (2013).

[9]A. Choudhury, A. K. Bhowmick, and C. Ong, *Polymer* **50**, 201 (2009).

[10]R. Rajasekar, K. Pal, G. Heinrich, A. Das, and C. K. Das, *Mat. Design* **30**, 3839 (2009).

[11]A. Das, R. Jurk, K. W. Stöckelhuber, and G. Heinrich, *eXPRESS Polym. Lett*. **1**, 717 (2007).

[12]S. Sadhu and A. K. Bhowmick, *J. Polym. Sci. Polym. Phys*. **42**, 1573 (2004).

[13]J.-T. Kim, D.-Y. Lee, T.-S. Oh, and D.-H. Lee, *J. Appl. Polym. Sci*. **89**, 2633 (2003).

[14]Y. T. Vu, J. E. Mark, L. H. Pham, and M. Engelhardt, *J. Appl. Polym. Sci*. **82**, 1391 (2001).

[15]I. Manas-Zloczower and D. L. Feke, *Int. Polym. Proc*. **4**, 3 (1989).

[16]R. I. Tanner and R. R. Huilgol, *Rheol. Acta*. **14**, 959 (1975).

[17]M. Tokihisa, K. Yakemoto, T. Sakai, L. A. Utracki, M. Sepehr, J. Li, and Y. Simard, *Polym. Eng. Sci*. **46**, 1040 (2006).

[18]W. L. Olbricht, J. M. Rallison, and L. G. Leal, *J. Non-Newt. Fluid Mech*. **10**, 291 (1982).

[19]C. M. Roland and M. Nguyen, *J. Appl. Polym. Sci*. **35**, 2141 (1988).

[20]J. L. Suter, D. Groen, and P. V. Coveney, *Nano Lett*. **15**, 8108 (2015).

[21]K. R. Paton, E. Varrla, C. Backes, R. J. Smith, U. Khan, A. O'Neill, C. Boland, M. Lotya, O. M. Istrate, P. King, T. Higgins, S. Barwich, P. May, P. Puczkarski, I. Ahmed, M. Moebius, H. Pettersson, E. Long, J. Coelho, S. E. O'Brien, E. K. McGuire, B. M. Sanchez, G. S. Duesberg, N. McEvoy, T. J. Pennycook, C. Downing, A. Crossley, V. Nicolosi, and J. N. Coleman, *Nat. Mat*. **13**, 624 (2014).

[22]L. Fang, M. Wei, N. Warasitthinon, J. Shen, R. Jian, D. Schmidt, C. Barry, and J. Mead, RUBBER CHEM. TECHNOL. **86**, 96 (2013).

[23]P.A. Small, *J. Appl. Chem*. **3**, 71 (1953).

[24]*Material Safety Data Sheets*, Southern Clay Products, Inc. and Akzo Nobel Chemicals, Inc.

[25]H. L. M. Hatharasinghe, M. V. Smalley, J. Swenson, G. D. Williams, R. K. Heenan, and S. M. King, *J. Phys. Chem. B* **102**, 6804 (1998).

[26]D. L. Ho and C. J. Glinka, *Chem. Mat*. **15**, 1309 (2003).

[27]R. A. Vaia and E. P. Giannelis, *Macromolecules* **30**, 7990 (1997).

[28]R. A. Vaia and E. P. Giannelis, *Macromolecules* **30**, 8000 (1997).

[29]C. M. Roland, J. K. Kallitsis, and K. G. Gravalos, *Macromolecules* **26**, 6474 (1993).

[30]P. Sotta, P.-A. Albouy, M. A. Taha, D. R. Long, P. Grau, C. Fayolle, and A. Papon, *Macromolecules* **50**, 6314 (2017).

[31]N. K. Borse and M. R. Kamal, *Polym. Eng. Sci*. **49**, 641 (2009).

[32]R. J. Stokes and D. F. Evans, *Fundamentals of Interfacial Engineering*, John Wiley & Sons, New York, 1997.

[33]J. Bandyopadhyay, S. S. Ray, M. Scriba, and J. Wesley-Smith, *Polymer* **55**, 2233 (2014).

[34]D. F. Bagster and D. Tomi, *Chem. Eng. Sci*. **29**, 1773 (1974).

[35]F. Bohin, I. Manas-Zloczower, and D. L. Feke, *Chem. Eng. Sci*. **51**, 5193 (1996).

[36]B. R. Bird, R. C. Armstrong, and O. Hassager, *Dynamics of Polymeric Liquids*, John Wiley and Sons, New York, 1987.

[37]C. K. Shih, *Polym. Eng. Sci*. **16**, 742 (1976).

[38]A. K. Panov, I. N. Dorokhov, T. V. Shulaeva, and V. V. Kafarov, *Doklady Adak. Nauk USSR* **301**, 155 (1988); *Doklady Adak. Nauk USSR* **322**, 560 (1992).

[39]G. Chen, S. Guo, and H. Li, *J. Appl. Polym. Sci*. **84**, 2451 (2002).

[40]Y. Z. Chen and H. L. Li, *J. Polym. Sci. Polym. Phys. Ed*. **45**, 1226 (2007).

[*Received January 2018, Revised May 2018*]